2020 IEEE International Conference on Robotics and Automation (ICRA)
31 May - 31 August, 2020. Paris, France

How far are Pneumatic Artificial Muscles from biological muscles?

Omid Mohseni[1,*], Ferréol Gagey[2], Gouping Zhao[3], Andre Seyfarth[3] and Maziar A. Sharbafi[1,3]

***Abstract*— There is a long history demonstrating humans' tendency to create artificial copies of living creatures. For moving machines called robots, actuators play a key role in developing human-like movements. Among different types of actuation, PAMs (pneumatic artificial muscles) are known as the most similar ones to biological muscles. In addition to similarities in force generation mechanism (tension based), the well-accepted argumentation from Klute et al., states that the PAM force-length (f_l) behavior is close to biological muscles, while the force-velocity (f_v) pattern is different. Using the multiplicative formulation of the pressure (as an activation term), f_l and f_v beside an additive passive parallel elastic element, we present a new model of PAM. This muscle-based model can predict PAM dynamic behaviors with high precision. With a second experiment on a two-segmented leg, the proposed model is verified to predict the generated forces of PAMs in an antagonistic arrangement. Such a dynamic muscle-like model of artificial muscles can be used for the design and control of legged robots to generate robust, efficient and versatile gaits.**

I. INTRODUCTION

Skeletal muscles in animals and humans can be considered as biological actuators which exert joint torques and generate movement. It has been shown that the intrinsic muscle properties (inherent compliance, i.e., muscle force-length and force-velocity relationships) play an important role in generating stable, robust and efficient locomotion behaviors [1-4]. Therefore, employing actuators with muscle-like properties in legged robotic systems can be beneficial.

In the current robotic systems, the McKibben type pneumatic artificial muscle (PAM) is one of the most widely used muscle-like actuators because of its simplicity and low-cost manufacturing [5], [6]. Compared to other types of actuators (i.e., electric motors and hydraulic actuators), PAMs provide more benefits in the conditions where high energy density, low added mass, almost no reflected inertia, and inherent compliance are required. For instance, in robotic legs [7], [8], robotic arms [9], [10], and exoskeletons [11-13].

A PAM is comprised of an inner rubber tube (expandable) surrounded by an outer mesh sheath (made from nonelastic Nylon fibers). It is rather difficult to build an accurate analytical PAM model because of the nonlinearity of force-length relationships in the rubber and the complex interaction forces between the inner tube and the outer mesh. A few static PAM models have been proposed based on the PAM working principles (energy conservation, virtual work) [14-17]. By adding friction components to the static model from [14], Tang and Liu developed a dynamic PAM model that described the PAM force as a high order polynomial function of pressure, contraction length and velocity, and external loads [18]. Sharbafi et al. [19] derived a dynamic PAM model by fitting a polynomial function to the measured data. The PAM force was modeled as a third-order polynomial function of PAM pressure, contraction length, and velocity [19]. All these models can describe the PAM behaviors to some extent, but there is no well-accepted PAM model that can accurately mimic the PAM dynamics and can be easily implemented in simulations. In addition, although the PAM has similar properties as biological muscles (e.g., tunable stiffness and inherent compliance), it remains unclear how far the PAM is from the biological muscle. Therefore, the goal of this study is to derive an accurate dynamic PAM model which has a similar structure as that of the biological muscle model (Hill-type [20]) so that we can investigate the similarities between the PAM and the biological muscle.

In this paper, we present a systematic approach to model PAMs as biological muscles and to identify the parameters. Then experimental studies are performed to verify the identified PAM models and evaluate their performance. Finally, the similarities between the PAM and the biological muscle are analyzed and discussed.

II. METHODS

A. PAM Identification Experiment

The experimental setup used in this study for identifying the PAM parameters is shown in Fig. 1. It is similar to the setup described in the previous study in [19]. It consists of a brushless DC motor (E8318-120KV, Hymotor, China), a PAM, and a force sensor (ALM-170, AMOS, Germany), all connected in series with non-stretchable Dyneema ropes. The PAM elongation was calculated by the motor angle and the radius of the pulley. The PAM air pressure was measured by an air pressure sensor (PSE 530, SMC, Japan). A Matlab xPC (2015b, Mathworks, USA) target machine was used to control the motor and collect data at 1 kHz.

In the PAM identification experiment, the PAM was first inflated to a certain initial pressure (with rope being slack). The initial pressure ranges from 200 kPa to 600 kPa. Then a force controller was applied to stretch the rope (desired force of 10 N). The motor encoder data in this condition were used to calculate the PAM rest length. Finally, the motor velocity was controlled with a randomized profile for 200 seconds.

[1]Omid Mohseni and Maziar A. Sharbafi are with School of ECE, Control and Intelligent Processing Center of Excellence (CIPCE), College of Engineering, University of Tehran, Tehran, Iran. o.mohseni,sharbafi@ut.ac.ir

[2]Ferréol Gagey is with École normale supérieure Paris-Saclay. ferreol.gagey@ens-paris-saclay.fr

[3]Gouping Zhao, Andre Seyfarth and Maziar A. Sharbafi are with Lauflabor Locomotion Lab, Centre for Cognitive Science, TU Darmstadt, Germany. zhao,seyfarth,sharbafi@sport.tu-darmstadt.de

∗ Corresponding author

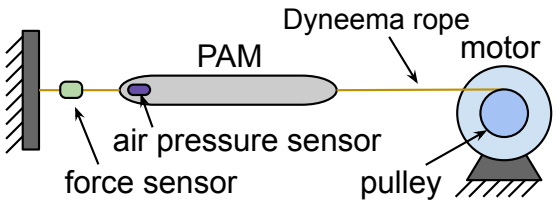

Fig. 1: Schematic of PAM identification experimental setup.

B. Muscle-like Modeling of PAM

Since PAMs offer characteristics like being light-weight and inherently compliant (due to the compressibility of air) and also due to their decreasing load-contraction relation, they are often regarded and referred to as human skeletal muscles. Though several research studies have attempted to model these actuators from different perspectives (e.g., geometrical, phenomenological, or empirical) [21], still to the best of our knowledge no well-accepted dynamic model has been proposed. In this study, we present a new dynamic model inspired by the muscle tendon complex model.

The key elements in the muscle modeling are Contractile Element (CE) and Elastic components in Series (SEC) or in Parallel (PEC). In the Hill-type muscle model [20], the generated force by the CE (F_{CE}) is given by:

$$F_{CE}\left(A, l_{CE}, v_{CE}\right) = A F_{max} f_l\left(l_{CE}\right) f_v\left(v_{CE}\right) \quad (1)$$

where A is the muscle activation level. In addition, l_{CE}, v_{CE} and F_{max} are the muscle length, contraction speed and maximum isometric force, respectively. For the force-length $f_l\left(l_{CE}\right)$ and the force-velocity $f_v\left(v_{CE}\right)$ relations, here we explain the equations introduced by [22].

$$f_l\left(l_{CE}\right) = \exp\left[c\left|\frac{l_{CE}-l_{opt}}{l_{opt}w}\right|^3\right] \quad (2)$$

where l_{opt} is the optimal CE length, w denotes the width of the bell-shaped $f_l\left(l_{CE}\right)$ curve and c is a constant value that can be considered as the muscle stiffness. The force-velocity $f_v\left(v_{CE}\right)$ is as follows:

$$f_v\left(v_{CE}\right) = \begin{cases} \dfrac{v_{max}-v_{CE}}{v_{max}+\kappa v_{CE}} & v_{CE} < 0 \\ N + (N-1)\dfrac{v_{max}+v_{CE}}{7.56\kappa v_{CE} - v_{max}} & v_{CE} \geq 0 \end{cases} \quad (3)$$

where, v_{max}, κ and N are constant values representing the maximum contraction velocity, the curvature constant and the eccentric force enhancement.

A quick glance at (1) shows that the CE force is in fact obtained by multiplication of four terms. It also reveals that the force is dependent on the length (l_{CE}) and velocity (v_{CE}). Motivated by this, we seek to find a similar relationship for describing the PAM force as a function of its related parameters. Among different combination of parallel and serial elastic elements for describing muscle behavior we found the combination of CE and PEC the most useful one to represent the PAM behavior [23].

$$F_{PAM}\left(P, l, v\right) = \underbrace{P F f_{la}\left(l\right) f_v\left(v\right)}_{Active} + \underbrace{F f_{lp}\left(l\right)}_{Passive} \quad (4)$$

where P, l and v denote the dependency of the PAM force on the instantaneous pressure, PAM length, and PAM velocity (i.e., rate of length variation), respectively. The parameter F is a constant playing the role of a fixed gain for the output PAM force; as in F_{max} in (1). Here, the active and passive parts represent the CE and PEC in biological muscles, respectively. The inner functions (f_l and f_v) in (4) are considered as follows:

$$\begin{aligned} f_{la}(l) &= 1 + a_0 l + a_1 l^2 + a_2 l^3 \\ f_v(v) &= 1 + b_0 v \\ f_{lp}(l) &= c_0 + c_1 l \end{aligned} \quad (5)$$

where $[a_0, a_1, a_2]$, $[b_0]$, and $[c_0, c_1]$ are unknown coefficients to be determined. It is also noteworthy to mention here that the above functions are selected based on the PAM measurement data, which will be discussed in more details in Section III. The form of the model proposed here in (4) reflects that the PAM dynamics is governed by an active part (CE) with P as the activation, and a passive part (PEC) working in parallel. Though other types of inner functions rather than polynomials may be used for f_l and f_v, these polynomials are found sufficient to provide accurate force estimation in later experiments.

C. Parameter Identification Protocol

The first step to identify the model parameters is to create training and testing sets of data. For that, we randomly split the experimental data to ensure that the training and testing sets are similar which in turn minimizes the effects of data discrepancies. Here, we divided the data into two sets: one with 75% of the source data, for training the model and one with 25% for testing. For calculating the coefficients $[a_0, a_1, a_2]$, $[b_0]$, $[c_0, c_1]$ and $[F]$ in (4), we used the `fminsearch` function in Matlab with random initial conditions. Of course, it should be noted here that other numerical optimization methods can be employed as well. Finally, for evaluating the performance of the fitted model, we inputted the testing dataset into the model and calculated the renowned R^2 coefficient of determination metric which is defined as:

$$R^2 = 1 - \frac{\sum_i \left(y_i - f_i\right)^2}{\sum_i \left(y_i - \bar{y}\right)^2} \quad (6)$$

where y_i and f_i denote the testing and estimated data samples, respectively. Also $\bar{y}$ is the mean of the testing dataset.

D. Verification Experiments

Identification of a model's unknown parameters based on a given set of data does not necessarily guarantee the correctness or accuracy of the model in face of every possible scenario. A comprehensive and well-identified model must

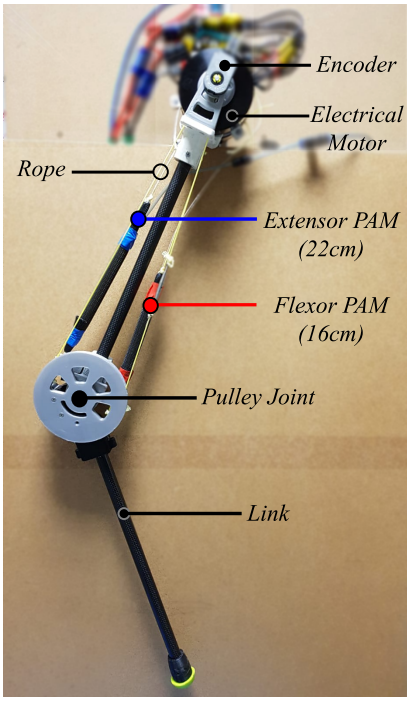

Fig. 2: Experimental setup used for verification of the PAMs.

then be applicable to other possible conditions and applications rather than just the one it is tuned for. In this regard, we tried to verify our proposed bioinspired PAM model (4) in a different experimental setup to provide supportive evidence for sufficiently accurate prediction of PAM behavior. For that, we installed two PAMs in an antagonistic arrangement on a joint of a two-link robot; see Fig. 2. As can be seen from this figure, a pair of PAMs denoted by *extensor* and *flexor* with lengths of 22 and 16 cm respectively are placed on a joint for actuation. The experiments for verifying the model are conducted in two cases: 1) the robot link is actuated by an electrical motor to move sinusoidally and the PAMs are inflated with a fixed amount of air pressure, and 2) the robot link is actuated directly by sinusoidal inflation/deflation of the PAMs and the motors are turned off.

III. RESULTS

A. PAM Identification

In order to identify the parameters of our model (4), we used the dataset from Subsection II-A. An insight into this dataset (for a PAM with a length of 16 cm) which is depicted in Fig. 3a shows the nonlinear dependency of PAM output force on its length, velocity and pressure. To better observe the relations between different PAM parameters which may not be clear in this 3D curve, one can refer to [19].

Using the training data and the proposed muscle-like PAM model (Eqs. 4 and 5) we predict the generated force for the testing data. The comparison between the experimental data and model prediction (for the PAM with 16 cm) is illustrated in Fig. 3b. The randomly zoomed area in this figure show that the model is well-fitted to the experimental data and thus the PAM parameters are identified correctly. Calculating the R^2 coefficient for this dataset also shows 98.12% correlation. It must be also noted here that the aforementioned evaluation process stated here was repeated for two other PAMs with different lengths (12 and 22 cm) and it was shown that fitting our muscle-like model (4) on PAMs yielded R^2 correlations of above 98%. The identified coefficients of the model for all of the three PAMs are summarized in Tab. I.

The general behavior of our PAM model with its considered polynomial inner functions (5) can be better understood by comparing it to the muscle inner functions in (2) and (3). For comparison, the values of muscle parameters are chosen commensurate with those reported in [24]. The normalized force-length graphs for both PAM and muscle are shown in Fig. 4a. For normalizing the PAM force-length relationship, we divided the length and force by their maximum values. This way the PAM force-length figure can be easily compared to that of muscle which is already normalized according to (2). However, it must be noted here that the muscle force-length is plotted only in the interval where it reaches its optimal length (i.e., l_{opt}). Now, it can be seen from Fig. 4a that the cubic polynomial considered for the PAM force-length mimics the rising edge of the muscle force-length, except the plateau at the end. In addition, Fig. 4b displays the force-velocity of PAM and muscle. Again here, the related graph for the PAM is normalized for comparison. An insight into this figure shows that the nonlinear force-velocity of the biological muscle is simplified to a linear relation in a limited range which is shown by the thick line. By performing identification tests in a wider range of circumstances, it can be expected that the behavioral patterns of our PAM model observed in here (either force-length or force-velocity relations) better mimic those of biological muscles.

B. PAM Verification

In order to evaluate our proposed PAM model and verify its accuracy, we conducted two experiments wherein two PAMs are located antagonistically on a joint; see Fig. 2. In the first experiment, both PAMs are inflated with a constant 500 kPa air pressure and the joint motor is moved sinusoidally while the PAM valves are closed entirely during the whole experiment; meaning no air pressure is let in or out. We then captured the joint angle, velocity, instantaneous pressure of the PAMs and also their force via the xPC target in Matlab, Simulink. Thereafter, these measurements were inputted into their corresponding PAM models to give us an estimate of the force. The experimental results are shown in Fig. 5. In this figure, the measured forces are compared with those of the model both for the extensor (Fig. 5a) and flexor (Fig. 5b). Calculating the R^2 metric yields 97.9% and 97.4% for the extensor and flexor forces, respectively; which indicates that the identified PAM models still hold for this experiment.

In the second experiment, however, the electrical motors were turned off and the PAMs were controlled in a sinusoidal manner with 500 kPa magnitude and 180 de-

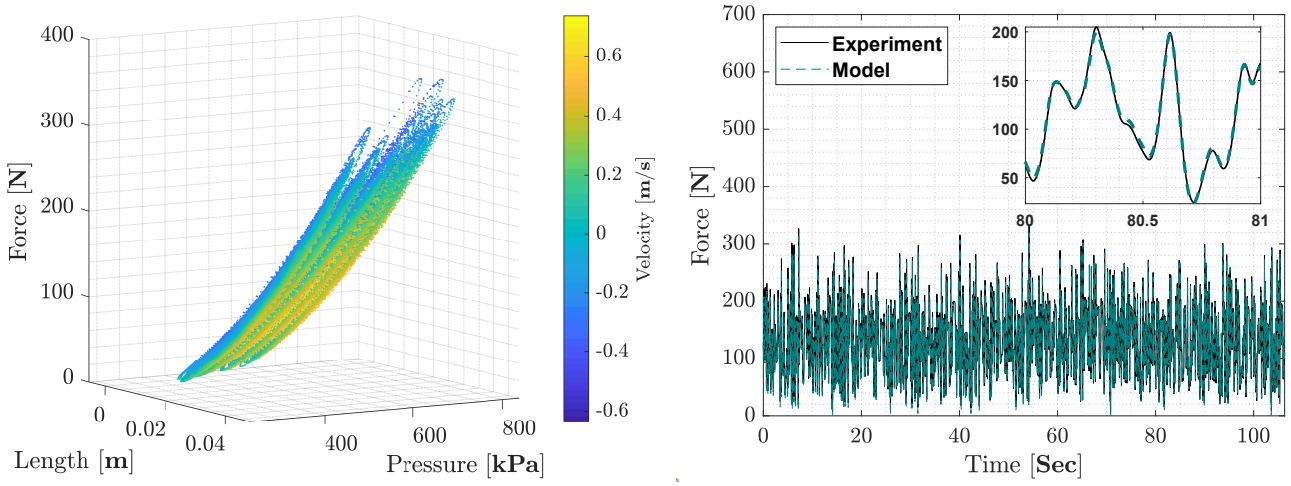

(a) (b)

Fig. 3: (a) Experimental data acquired from the PAM identification experiments in different initial pressures (ranging from 200 to 600 kPa) for a PAM with the length of 16 cm. (b) Real PAM force versus PAM output force from modeling. An interval of one second is zoomed here for illustration purposes and better comparison.

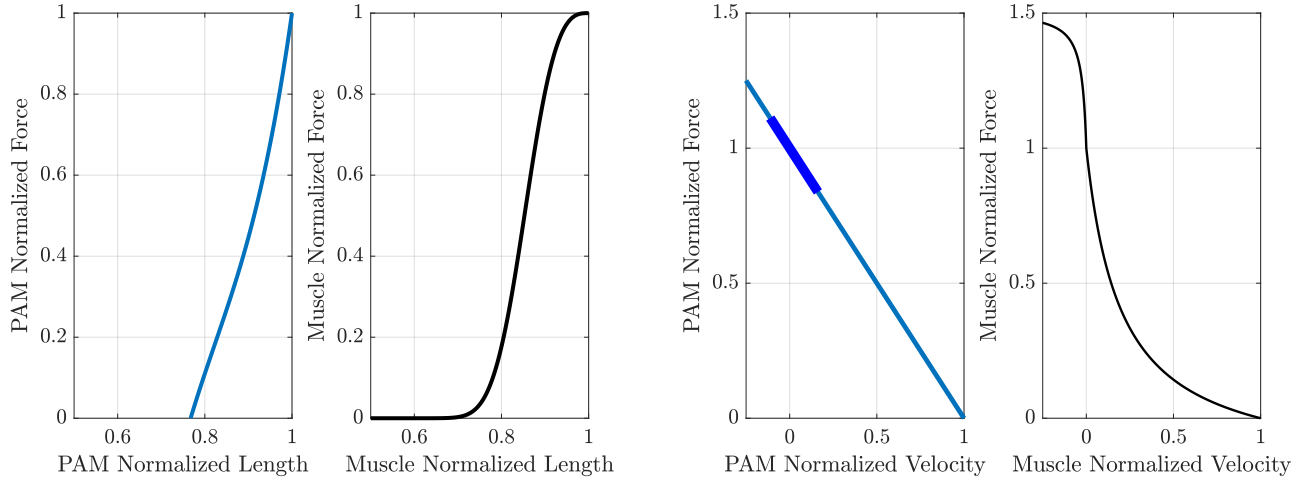

(a) (b)

Fig. 4: Comparison between muscle and PAM in terms of force-length and force-velocity dependency.

TABLE I: Identified model parameters of PAMs

	F	a_0	a_1	a_2	b_0	c_0	c_1
PAM (22cm)	0.3235	16.99	-298	3600	-0.16	-592.32	6430
PAM (16cm)	0.2849	25.22	-267	7600	-0.22	-499.54	7488
PAM (12cm)	0.1562	104.93	-2064	80500	-0.36	-482.38	6338

gree phase difference. The frequency was also set to 1 Hz. Needless to say, as a result of such actuation, the robot joint moves sinusoidally. For conducting this experiment, each PAM was equipped with two continuous valves (PVQ-series proportional solenoid valves), one for supplying the air pressure and one for exhausting it. Then, PAMs were PID controlled using the pressure measurements as feedback variables. Fig. 6 illustrates the results obtained from this experiment and it shows that the model's estimated force acceptably resemble the measured force both in terms of pattern and magnitude, which in turn shows the validity of our model. The discrepancies between the model and

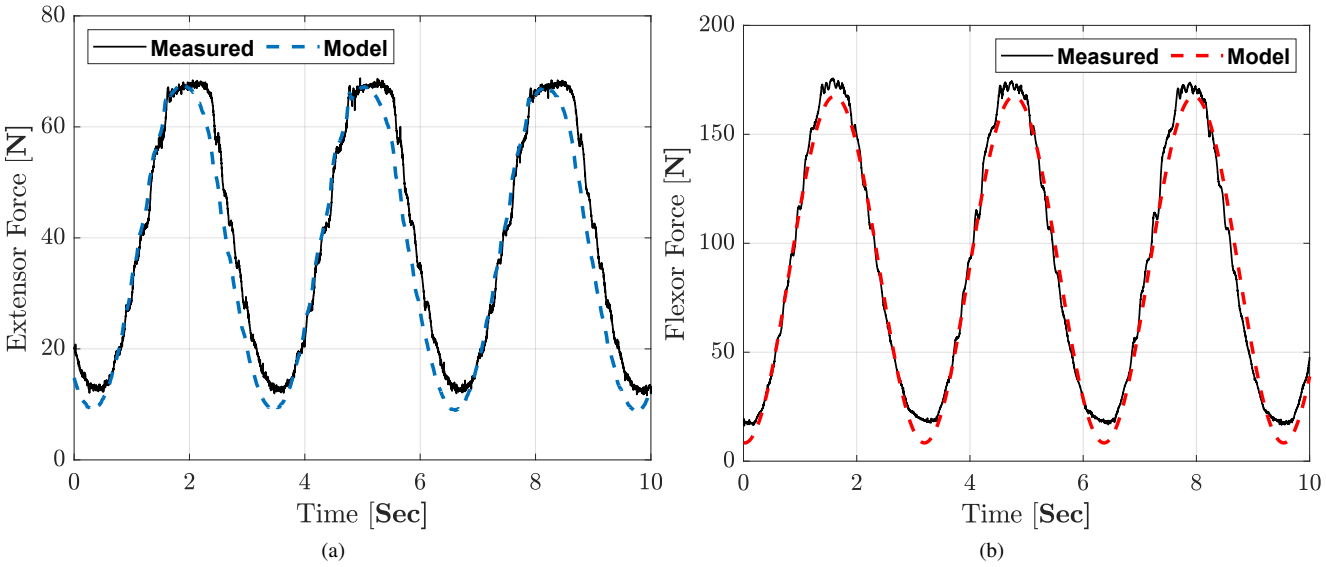

Fig. 5: Comparison of PAMs' measured forces with PAM model during sinusoidal movements of the robot link by means of an electrical motor. (a) shows the results for the extensor and (b) displays the force for the flexor PAM.

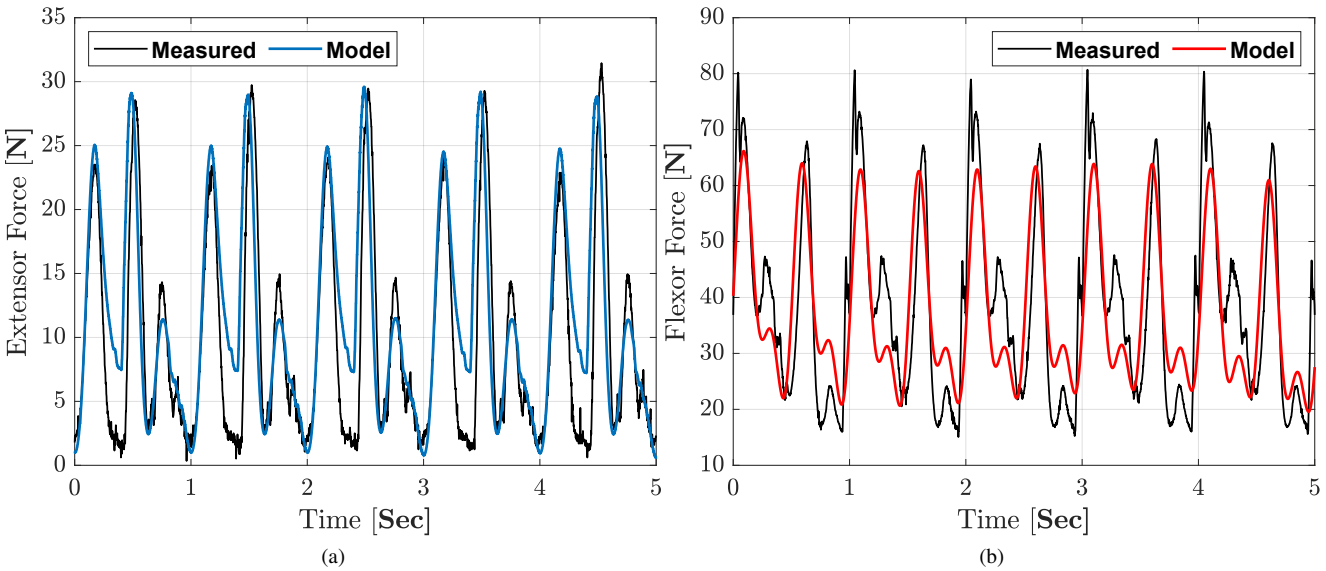

Fig. 6: Comparison of the measured force of the PAMs with the force outputted from our PAM model during an antagonistic actuation experiment of the PAMs. (a) shows the results for the extensor and (b) displays the force for the flexor PAM.

experimental results observed in here are due to the fact that the PAMs' identification experiments (Subsection II-A) were performed with constant amount of air pressures inside the PAMs. Overall, according to the obtained experimental outcomes, it can be concluded that our proposed bioinspired PAM model (4) is well-identified and accurate for cases where the amount of air pressure inside the PAM is kept constant, and it works acceptably in other practical scenarios with variable pressure, as in the second experiment.

IV. DISCUSSIONS

In this study, we introduced a new perspective in understanding the PAM (pneumatic artificial muscle) behavior in light of our knowledge about biological muscle properties. Different models have been developed for explaining biological muscle behaviors and they are all comprised of contractile and passive elastic elements [25], [26]. In our empirical investigations, we also found that a CE (contractile element) beside a PEC (parallel elastic component) can better predict the PAM dynamics compared to previous studies. This bioinspired model plus a serial tendon could better approximate biological muscle behaviors [27].

With the proposed combination of active (CE) and passive (PEC) elements, different behavioral patterns can be better understood. This way, the identified force-length and force-

velocity relations of the active part were better represented. Here, the similarity between the biological and artificial muscle models is twofold: 1) structural level and 2) control level when they are considered as tunable impedance.

Similarity in structural level: The results show that multiplication of different functions of force versus velocity and length, and the injected pressure as the activation signal is crucial to understand the artificial muscle behavior. Previous studies on developing models by considering combinations of different functions of pressure, length and velocity [19], [28] never described separate spring or damper like behaviors of the PAMs. From this viewpoint, multiplicative formulation and increasing and decreasing relations, respectively, for force-length and force-velocity with comparable patterns to biological muscles are two important features of PAMs in the structural level. The introduced formulation (4) is the key to expose the underlying dynamical behavior of PAMs. This way the presented model can predict the second (verification) experimental results. Despite the general patterns of the f_l and f_v in PAMs which are comparable with their biological counterparts, the most significant difference is the smaller damping effect in the PAM compared to muscles. These outcomes are in line with findings of Klute et al. [29].

Control level: Similar to the activation signal in biological muscles, air pressure can be considered as an input signal to tune these muscles' impedance. Multiplication of the activation signal with the intrinsic behaviors of the muscles enable the system to be considered as variable impedance actuators [30]. This property is very useful for locomotion control. Recently, PAMs are employed as variable compliances in a hybrid actuation design called EPA (electric-pneumatic actuator) [19]. More recent studies presented theoretical methods to design parallel compliances for increasing efficiency and robustness in locomotion [31], [32]. With our proposed model, PAMs can be utilized to design the required impedance for increasing efficiency and robustness supported by stability analyses.

Based on the proposed model, we also implemented a Simulink model of PAM as a new actuator block. In this model, for each length and velocity (of the PAM) calculated by the kinematic relations, and the injected amount of air, the force F_{PAM} is calculated. If the valves are closed, the instantaneous pressure can be also estimated based on a similar formulation to be set as another input in actuator block. The developed PAM Simulink model can be used for further simulations in the future.

Since in the identification experiment, the valves were closed, we did not expect to precisely predict the experimental results while air flow changes the amount of air inside the PAMs and consequently the dynamic behavior. For this reason, the prediction precision of the experiments with closed valves (Fig. 5) was better than that of with controlled valves (Fig. 6). However, with such a fundamental difference our model capability in prediction of the PAM behavior is noticeable. In the future, identification experiments with controlled valves could further improve the model.

V. ACKNOWLEDGMENT

The authors would like to thank Mitsuhiro Yabu and Prof. Koh Hosoda (Osaka University) for supporting us to develop the experimental setup and also thank Ayoob Davoodi (University of Tehran) for his helpful discussions. This research is supported by the DFG-Funded EPA Project under Grant AH307/2-1 and Grant SE1042/29-1.

REFERENCES

[1] Karin GM Gerritsen, Anton J van den Bogert, Manuel Hulliger, and Ronald F Zernicke. Intrinsic muscle properties facilitate locomotor controla computer simulation study. *Motor control*, 2(3):206–220, 1998.

[2] Monica A. Daley, Alexandra Voloshina, and Andrew A. Biewener. The role of intrinsic muscle mechanics in the neuromuscular control of stable running in the guinea fowl. *The Journal of Physiology*, 587(11):2693–2707, 2009.

[3] D F B Haeufle, S Grimmer, and A Seyfarth. The role of intrinsic muscle properties for stable hopping—stability is achieved by the force–velocity relation. *Bioinspiration & Biomimetics*, 5(1):016004, feb 2010.

[4] Ayoob Davoodi, Omid Mohseni, Andre Seyfarth, and Maziar A Sharbafi. From template to anchors: transfer of virtual pendulum posture control balance template to adaptive neuromuscular gait model increases walking stability. *Royal Society open science*, 6(3):181911, 2019.

[5] Bertrand Tondu. Modelling of the mckibben artificial muscle: A review. *Journal of Intelligent Material Systems and Structures*, 23(3):225–253, 2012.

[6] Daniela Rus and Michael T. Tolley. Design, fabrication and control of soft robots. *Nature*, 521:467–475, 05 2015.

[7] Koh Hosoda, Takashi Takuma, Atsushi Nakamoto, and Shinji Hayashi. Biped robot design powered by antagonistic pneumatic actuators for multi-modal locomotion. *Robotics and Autonomous Systems*, 56(1):46 – 53, 2008. Human Technologies: Know-how.

[8] K. Ogawa, K. Narioka, and K. Hosoda. Development of whole-body humanoid pneumat-bs with pneumatic musculoskeletal system. In *2011 IEEE/RSJ International Conference on Intelligent Robots and Systems*, pages 4838–4843, Sep. 2011.

[9] B. Tondu, S. Ippolito, J. Guiochet, and A. Daidie. A seven-degrees-of-freedom robot-arm driven by pneumatic artificial muscles for humanoid robots. *The International Journal of Robotics Research*, 24(4):257–274, 2005.

[10] Festo airic's arm. https://www.festo.com/group/en/cms/10247.htm.

[11] M. Wehner, B. Quinlivan, P. M. Aubin, E. Martinez-Villalpando, M. Baumann, L. Stirling, K. Holt, R. Wood, and C. Walsh. A lightweight soft exosuit for gait assistance. In *2013 IEEE International Conference on Robotics and Automation*, pages 3362–3369, May 2013.

[12] Yong-Lae Park, Bor rong Chen, Néstor O Pérez-Arancibia, Diana Young, Leia Stirling, Robert J Wood, Eugene C Goldfield, and Radhika Nagpal. Design and control of a bio-inspired soft wearable robotic device for ankle–foot rehabilitation. *Bioinspiration & Biomimetics*, 9(1):016007, jan 2014.

[13] Philippe Malcolm, Samuel Galle, Wim Derave, and Dirk De Clercq. Bi-articular knee-ankle-foot exoskeleton produces higher metabolic cost reduction than weight-matched mono-articular exoskeleton. *Frontiers in neuroscience*, 12:69–69, 03 2018.

[14] Ching-Ping Chou and B. Hannaford. Measurement and modeling of mckibben pneumatic artificial muscles. *IEEE Transactions on Robotics and Automation*, 12(1):90–102, Feb 1996.

[15] N. Tsagarakis and D. G. Caldwell. Improved modelling and assessment of pneumatic muscle actuators. In *Proceedings 2000 ICRA. Millennium Conference. IEEE International Conference on Robotics and Automation. Symposia Proceedings (Cat. No.00CH37065)*, volume 4, pages 3641–3646 vol.4, April 2000.

[16] B. Tondu and P. Lopez. Modeling and control of mckibben artificial muscle robot actuators. *IEEE Control Systems Magazine*, 20(2):15–38, April 2000.

[17] M. Doumit, A. Fahim, and M. Munro. Analytical modeling and experimental validation of the braided pneumatic muscle. *IEEE Transactions on Robotics*, 25(6):1282–1291, Dec 2009.

[18] Ruiyi Tang and Dikai Liu. An enhanced dynamic model for mckibben pneumatic muscle actuators. In *Proceedings of the Australasian Conference on Robotics and Automation, Wellington, NZ, USA*, pages 3–5, 2012.

[19] Maziar Ahmad Sharbafi, Hirofumi Shin, Guoping Zhao, Koh Hosoda, and Andre Seyfarth. Electric-pneumatic actuator: A new muscle for locomotion. In *Actuators*, volume 6, page 30. Multidisciplinary Digital Publishing Institute, 2017.

[20] AV Hill. The heat of shortening and the dynamic constants of muscle. *Proceedings of the Royal Society of London B: Biological Sciences*, 126(843):136–195, 1938.

[21] Eleni Kelasidi, George Andrikopoulos, George Nikolakopoulos, and Stamatis Manesis. A survey on pneumatic muscle actuators modeling. In *2011 IEEE International Symposium on Industrial Electronics*, pages 1263–1269. IEEE, 2011.

[22] Xavier Aubert. *Le Couplage énergétique de la contraction musculaire, par Xavier Aubert. Thèse...* Editions Arscia, 1956.

[23] Koh Hosoda, Christian Rode, Tobias Siebert, Bram Vanderborght, Maarten Weckx, and D Lefeber. Actuation in legged locomotion. In *Bioinspired Legged Locomotion*, pages 563–622. Elsevier, 2017.

[24] Hartmut Geyer, Andre Seyfarth, and Reinhard Blickhan. Positive force feedback in bouncing gaits? *Proceedings of the Royal Society of London. Series B: Biological Sciences*, 270(1529):2173–2183, 2003.

[25] A. J. "Knoek" van Soest, Wouter P. Haenen, and Leonard A. Rozendaal. Stability of bipedal stance: the contribution of cocontraction and spindle feedback. *Biological Cybernetics*, 88(4):293–301, 2003.

[26] Gertjan JC Ettema and Kenneth Meijer. Muscle contraction history: modified hill versus an exponential decay model. *Biological Cybernetics*, 83(6):491–500, 2000.

[27] Tobias Siebert, Christian Rode, Walter Herzog, Olaf Till, and Reinhard Blickhan. Nonlinearities make a difference: comparison of two common hill-type models with real muscle. *Biological cybernetics*, 98(2):133–143, 2008.

[28] Ching-Ping Chou and Blake Hannaford. Measurement and modeling of mckibben pneumatic artificial muscles. *IEEE Transactions on robotics and automation*, 12(1):90–102, 1996.

[29] Glenn K Klute, Joseph M Czerniecki, and Blake Hannaford. Mckibben artificial muscles: pneumatic actuators with biomechanical intelligence. In *1999 IEEE/ASME International Conference on Advanced Intelligent Mechatronics (Cat. No. 99TH8399)*, pages 221–226. IEEE, 1999.

[30] Bram Vanderborght, Alin Albu-Schäffer, Antonio Bicchi, Etienne Burdet, Darwin G Caldwell, Raffaella Carloni, MG Catalano, Oliver Eiberger, Werner Friedl, Ganesh Ganesh, et al. Variable impedance actuators: A review. *Robotics and autonomous systems*, 61(12):1601–1614, 2013.

[31] M. A. Shahri, O. Mohseni, H. J. Bidgoly, and M. N. Ahmadabadi. Profile design of parallel rotary compliance for energy efficiency in cyclic tasks. *IEEE/ASME Transactions on Mechatronics*, 25(1):142–151, Feb 2020.

[32] M. A. Sharbafi, M. J. Yazdanpanah, M. N. Ahmadabadi, and A. Seyfarth. Parallel compliance design for increasing robustness and efficiency in legged locomotionproof of concept. *IEEE/ASME Transactions on Mechatronics*, 24(4):1541–1552, 2019.